Antiphase OH and OI airglow emissions induced by a short-period ducted gravity wave

Jonathan B. Snively and Victor P. Pasko

Communications and Space Sciences Laboratory (CSSL), Department of Electrical Engineering, Pennsylvania State University, University Park, Pennsylvania, USA

Received 13 December 2004; revised 28 January 2005; accepted 25 March 2005; published 22 April 2005.

[1] Numerical simulation of a ducted gravity wave event suggests that OH (8,3) and O(^{1}S) 557.7 nm airglow emissions layers may exhibit opposite-phase intensities when perturbed by a short-period wave undergoing vertical reflection. This effect arises due to the time and temperature dependance of the OH excitation reaction, coupled with the linear polarization properties of vertically-standing waves. **Citation:** Snively, J. B., and V. P. Pasko (2005), Antiphase OH and OI airglow emissions induced by a short-period ducted gravity wave, *Geophys. Res. Lett.*, *32*, L08808, doi:10.1029/2004GL022221.

1. Introduction

[2] Following the ALOHA93 campaign, *Taylor et al.* [1995] reported a ''spectacular gravity wave event'' observed on October 10th, 1993. A wave with $\tau \simeq$ 4.4 min period and $\lambda_x \simeq 20$ km horizontal wavelength was observed to propagate into a region of depleted hydroxyl (OH) emissions and enhanced atomic oxygen (OI) emissions. As the wave passed, a jump in OH background intensity and decrease in OI background intensity was observed, and wave intensity perturbations appeared in antiphase between the two airglow layers, such that bright regions of OH corresponded with dark regions of OI and vice-versa. A previous event, observed on October 9th, 1993 and reported by *Swenson and Espy* [1995], exhibited similar large-scale but less-pronounced small-scale structure. It was found consistent with a $\lambda_x = 350$ km propagating wave with $\lambda_z = 20$ km, 75 m/s horizontal phase velocity, and a dynamic phase reversal between OI and OH airglow layers [*Swenson et al.*, 1998].

[3] Three years following the publication of *Taylor et al.* [1995], two interpretations for the observed short-period wave were proposed:

[4] *Munasinghe et al.* [1998] proposed that the short-period wave could be explained by a fully-ducted gravity wave, with wave spectral characteristics determined by the duct mode and antiphase airglow perturbations resulting from a waveguide node present between OH and OI emissions layers (dynamic phase reversal). Alone, this interpretation does not provide an explanation for the observed background intensity jumps, or a mechanism for the generation of the short-period wave.

[5] *Dewan and Picard* [1998] suggested that the wave resulted from the passage of a mesospheric bore. By this interpretation, the wave would result from the dissipation and dispersion of a front-like structure propagating in a stable inversion layer. The phase differences between OH and OI emissions would correspond with upward and downward displacements associated with the passage of the bore. Observed background intensity jumps are then assumed to arise from the bore's bulk perturbation.

[6] Both explanations assume a wave inside a stable atmospheric duct and rely on a wave-dynamic phase differences to explain the antiphase OH and OI airglow emissions. The phase reversal reported by *Taylor et al.* [1995] is not unique; *Smith et al.* [2003] also documented a similar wave event in which short-period wave-induced OH and OI airglow perturbations were distinctly antiphase.

[7] Due to varying chemical processes, different airglow layers may react differently given identical wave perturbations. It was found by *Hines and Tarasick* [1994] that vertically standing or evanescent waves ($k_z \rightarrow 0$) may induce airglow perturbations with a phase of 0° or 180° with respect to the wave temperature perturbation; it was also noted that intermediate phase variations ($0° < \phi < 180°$) may arise given photochemical processes occurring over time scales comparable to a wave period. Airglow phase variations (between temperature and intensity or between intensity of different emissions layers) are also of importance for waves with smaller vertical wavelength and for freely propagating and damped waves [*Swenson and Gardner*, 1998; *Liu and Swenson*, 2003]. In this paper we will concentrate our discussion on small-scale waves that are well-within the evanescent/ducted regime.

[8] Airglow perturbations for the ducted wave predicted by *Munasinghe et al.* [1998] have been modeled by *Makhlouf et al.* [1998]. Results suggest significant phase variations between the OH and OI emissions intensities and the temperature perturbation; however, the model explicitly assumed waveguide nodes between the airglow layers, adding a degree of further complexity. It is noted by *Makhlouf et al.* [1998] that the chemical lifetimes of OI and its precursors are on the order of several seconds, while the lifetime of O_3 consumed in the excitation reaction leading to OH is on the order of 10 min. It follows that, in agreement with predictions by *Hines and Tarasick* [1994], the OI intensity perturbation exhibited 0° or 180° phase between the intensity and temperature perturbations, while the strongly time-dependent OH emission exhibited intermediate phase variations ($0° < \phi < 180°$). Whether or not results presented by *Makhlouf et al.* [1998] could explain the antiphase OH and OI airglow signature observed by *Taylor et al.* [1995] is obscured by the multi-node ducted wave model, as the position of nodes and duct boundaries will strongly influence the solution.

0094-8276/05/2004GL022221$05.00

[9] The purpose of this paper is to examine the ducting interpretation of *Munasinghe et al.* [1998] using a fully-nonlinear numerical model coupled with simple airglow chemistry models. For our study, however, we will use the wave-breaking mechanism of *Snively and Pasko* [2003] to excite a ducted wave resembling that proposed by *Munasinghe et al.* [1998] and will examine how such a wave would influence the hydroxyl (OH vibrational (8,3)) and atomic oxygen (OI 557.7) airglow layers.

2. Model Formulation

[10] The employed numerical model is 2-D, nonlinear, inviscid, compressible, and non-rotating [*Snively and Pasko*, 2003]. It is based on a flux limited, finite volume method developed by *LeVeque* [2002] and implemented in the CLAWPACK software package (http://www.amath.washington.edu/~claw). The simulation domain extends from ground to an altitude of 220 km, and has a horizontal extent of 1800 km with uniform vertical and horizontal grid resolutions Δ_z = 1 km and Δ_x = 1 km, respectively. Boundary conditions are identical to those used by *Snively and Pasko* [2003]. The source of the gravity waves is positioned at x_o = 450 km and z_o = 12 km (i.e., 450 km from the left boundary of the simulation domain and at 12 km altitude). It is a mechanical oscillator providing a vertical force at a chosen frequency (ω) and horizontal wavenumber (k_x) of the form $\sim\exp[-(x - x_o)^2/2\sigma_x^2 - (z - z_o)^2/2\sigma_z^2 - (t - t_o)^2/2\sigma_t^2]\cos[k_x x]\cos[\omega t]$, where σ_x and σ_z are the Gaussian envelope's horizontal and vertical half-widths, respectively, and σ_t is the temporal Gaussian half-width; the position given by x_o, z_o, and t_o corresponds to the source maximum in space and time.

[11] To approximate the background atmospheric structure present for the event reported by *Taylor et al.* [1995], we use data obtained for October 10, 1993, at 10:30 LT, for a geographical latitude 20.8° and longitude 203.8° from the MSIS-E-90 model [*Hedin*, 1991] (http://nssdc.gsfc.nasa.gov/space/model/atmos/msise.html). The model also provides major and minor species concentrations for O, O_2, N_2, and H.

[12] Prior to simulation, an analytic solution was used to calculate constant horizontal wind velocity u to yield a ducted gravity wave mode resembling the *Taylor et al.* [1995] event and *Munasinghe et al.* [1998] prediction. It was found that a 10.5 m/s flow would yield a fully-ducted, 2-node, wave mode with 4.4 min period and 20 km wavelength. This is consistent with the observed 10–17 m/s wind along the direction of wave propagation as measured by J. R. Isler (cited as private communication in work by *Taylor et al.* [1995]). Source wave magnitude is chosen such that breaking will only occur for peak magnitudes of the Gaussian forcing. Breaking is concentrated above mesopause and inside the duct, with vertical velocities of the primary wave reaching a few m/s at airglow altitudes and a few tens of m/s at the top of the duct. The modeled duct comprises the altitude region from ~90–130 km for the chosen wave parameters and wind velocity. Several nonlinear processes may contribute to the formation of secondary waves inside the duct, including those associated with wavebreaking [e.g., *Snively and Pasko*, 2003, and references therein] and with the passage of the source wave [*Chimonas et al.*, 1996]. These nonlinear mechanisms predict the generation of secondary waves with approximately doubled frequency and horizontal wavenumber (τ/2 and λ_x/2). Simulation parameters are chosen to excite a source wave with period τ = 8.8 min and horizontal wavelength λ_x = 40 km, which is twice the period and horizontal wavelength of the wave reported by *Taylor et al.* [1995]. Secondary waves should thus agree with modal solutions predicted by *Munasinghe et al.* [1998], and are notably weaker than the breaking primary wave and remain linear throughout the duct [e.g., *Snively and Pasko*, 2003].

[13] The present study assumes constant flow, and duct structure that arises primarily from thermal variations. During the review process, G. R. Swenson noted the possibility that a long-period wave, such as that reported by *Swenson and Espy* [1995], may induce large-scale airglow intensity changes similar to those reported by *Taylor et al.* [1995]. This possibility also raises questions as to how a propagating large-scale wave could influence the generation, propagation and ducting of the observed short-period wave, which will be addressed in a future study.

[14] The airglow layers that we wish to model arise from the atomic oxygen O(^{1}S) 557.7 nm and hydroxyl OH(v = 8,3) NIR emissions. Wave-induced perturbations are introduced through temperature-dependent reaction rates and chemical species density variations. Atomic oxygen O is conservatively advected at the fluid velocity to obtain [O] and major species densities ([O_2], [N_2]) are assumed to be proportional to ρ/ρ_o, where ρ_o is the background density at a specific altitude, $\hat{\rho}$ is the wave-induced density perturbation, and $\rho = \hat{\rho} + \rho_o$.

[15] The O(^{1}S) emission peaks near 96 km and arises from a two-step reaction sequence involving an excited state (O_2^*) as a precursor [e.g. *McDade et al.*, 1986]:

$$O + O + M \xrightarrow{k_0} O_2^* + M \tag{1}$$

$$O_2^* + O \rightarrow O(^1S) + O_2 \tag{2}$$

The model of *McDade et al.* [1986] and *Murtagh et al.* [1990] assumes that the precursor involved in the reaction is an unknown excited state of O_2. Airglow calculations are performed using a steady-state model for the OI emission. The OI emission is determined by the empirical model given by *McDade et al.* [1986] and *Murtagh et al.* [1990]. This model has been recently used by *Horinouchi* [2004] to study instability structures in airglow. The photon volume emission rate V_{OI} (cm^{-3}s^{-1}) for the OI 557.7 nm emission is:

$$V_{OI} = \frac{A_5 k_0 [O]^3 \{[N_2] + [O_2]\}}{\{A_6 + k_5[O_2]\}\{C'^{O_2}[O_2] + C'^{O}[O]\}} \tag{3}$$

where A_5 and A_6 are Einstein coefficients, $k_5 = 4.0 \times 10^{-12}\exp(-865/T)$ (cm^{3}s^{-1}) is the quenching rate of O(^{1}S) due to molecular oxygen. Coefficients C'^{O_2} and C'^{O} are empirically determined parameters describing the excitation process [*Murtagh et al.*, 1990], which are valid under the assumption that the precursor is a product of the three-body recombination of atomic oxygen. The rate coefficient

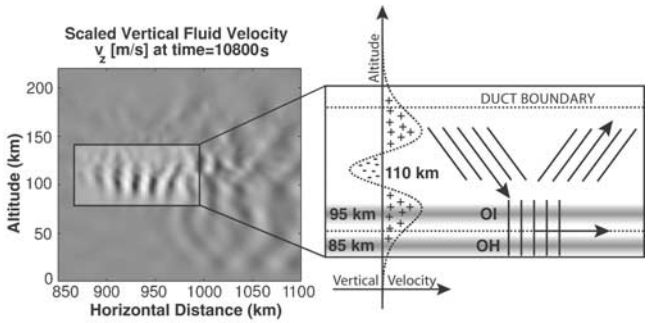

Figure 1. Normalized vertical velocity taken at t = 10,800 sec with schematic illustration of duct phase variations; wave reflection and evanescence occurs in the vicinity of both OH and OI airglow layers.

of this reaction is given by $k_0 = 4.7 \times 10^{-33}(300/T)^2$ (cm^6s^{-1}), which exhibits negative temperature dependence such that the rate decreases for increasing temperature (with T in degrees Kelvin) [*Murtagh et al.*, 1990].

[16] The OH emission peaks near 87 km altitude and arises from the reaction:

$$H + O_3 \xrightarrow{k_1} OH(v) + O_2 \tag{4}$$

However, the reaction leading to the production of O_3 is also of relevance:

$$O_2 + O + M \xrightarrow{k_6^{N_2,O_2}} O_3 + M \tag{5}$$

The OH vibrational excitation reaction is a dominant loss process for O_3 and, under steady-state conditions, the unperturbed OH emission rate can be estimated from the O_3 production rate.

[17] The OH emission rate is calculated using a variation on the "sudden death" model of *McDade et al.* [1987], which was later adapted by *Swenson and Gardner* [1998] and used by *Liu and Swenson* [2003]. The lifetime of OH(v) is very short with respect to a wave period, so we assume that the emission process is in steady-state [*McDade et al.*, 1987]. Production of OH(v) is the dominant loss process for O_3, which has a lifetime on the order of a wave period (~6–10 min). We thus allow for time-dependence of $[O_3]$, following dynamics of O_3 in time starting from initial steady-state conditions. The volume emission rate for NIR photons $V_{OH(8,3)}$ ($cm^{-3}s^{-1}$) is given by:

$$V_{OH(8,3)} = \frac{A(8,3)k_1[H][O_3]f(8)}{L(8)} \tag{6}$$

$$\frac{\partial[O_3]}{\partial t} = \left(k_6^{N_2}[N_2] + k_6^{O_2}[O_2]\right)[O_2][O] - k_1[H][O_3] - \nabla\cdot([O_3]\vec{v}) \tag{7}$$

where $A(8,3)$, $f(8)$, $L(8)$ are the Einstein coefficient, fraction of emission due to the $v = 8$ excited state, and an empirical loss term, respectively; these, along with reaction rates $k_6^{N_2}$ and $k_6^{O_2}$, are given by *McDade et al.* [1987] and *Swenson and Gardner* [1998]. Dynamic transport of O_3 is included explicitly in the numerical solution of (7). For (4), we use the temperature-dependent rate coefficient of *Makhlouf et al.* [1995] $k_1 = 1.4 \times 10^{-10}\exp(-470/T)$ (cm^3s^{-1}), describing production of OH(v) with vibrational states v = 6–9, where a fraction equal to $f(8) = 0.27$ correspond to the $v = 8$ state.

3. Results and Discussion

[18] Figure 1 shows results of model calculations at t = 10,800 sec for source parameters $\omega = 0.0119$ rad/sec (τ = 8.8 min), $k_x = 0.000157$ rad/m (λ_x = 40 km), σ_x = 30 km, σ_z = 4 km, and σ_t = 10 min. The quantity presented in Figure 1 is the normalized vertical velocity $w_z = (\rho_o/\rho_s)^{1/2}v_z$, where ρ_s and ρ_o are atmospheric neutral mass densities at Earth's surface and at an altitude z, respectively.

[19] As schematically shown in Figure 1, the ducted wave mode has two nodes; however, the lowest node exists at an altitude above the OI airglow layer. The ducted wave is reaching evanescence at altitudes between the OH and OI airglow layers and is perturbing both layers with no significant dynamic phase differences. While the possibility of a dynamic phase reversal between airglow layers was suggested by *Munasinghe et al.* [1998], we do not observe this in our simulation.

[20] Figure 2b shows the OI and OH volume emissions rates integrated over vertical line of sight between 0 and 220 km altitudes to yield units $cm^{-2}s^{-1}$. Figure 2c shows the OI and OH integrated emission rates for the modeled case reported by *Snively and Pasko* [2003] for a zero-node ducted wave with vertical structure in the airglow layers. It is evident from Figures 2b and 2c that the OH integrated emission is 180° out of phase with the OI emission. This phase difference strongly resembles that associated with gravity wave events characterized as mesospheric bores; the modeled results do not, however, reproduce the background intensity jumps observed by *Taylor et al.* [1995] and *Smith et al.* [2003].

[21] The OI excitation and emission occurs on a timescale much less than a gravity wave period. The volume emis-

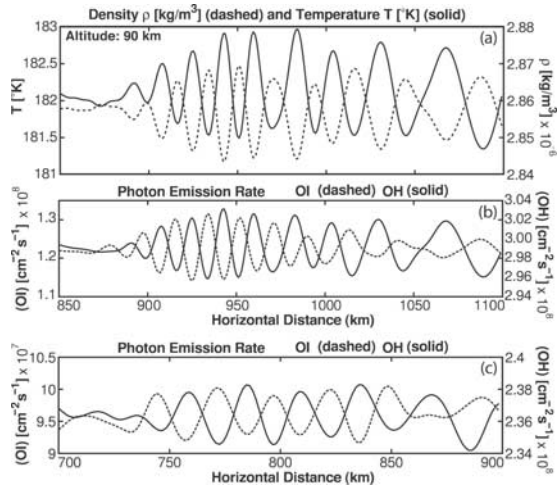

Figure 2. (a) Density (dashed) and temperature (solid) taken at t = 10,800 sec for 90 km altitude slice. (b) Integrated photon emission rates for OI (dashed) and OH (solid) airglow emissions and (c) OI (dashed) and OH (solid) airglow emissions for 5 min, zero-node wave from *Snively and Pasko* [2003].

sions rate given by (3) increases with positive perturbations of atomic oxygen density [O] and negative perturbations of temperature ($k_0\uparrow$, $k_5\downarrow$ for $T\downarrow$). For a vertically standing wave with frequency higher than $\omega \simeq 0.837N$, where N is the Brunt-Väisälä frequency, the wave's velocity perturbation is vertically polarized ($v_z \gg v_x$). For high-frequency ($\omega > 0.837N$) vertical waves, polarization relations [e.g., *Hines and Tarasick*, 1994] predict that density and temperature perturbations will be in antiphase; this prediction is confirmed by the simulation. The simulated wave-induced perturbations of OI emission intensity are 180° out of phase with the temperature perturbations, and in phase with the density perturbations (Figures 2a and 2b). The 180° phase shift between temperature and OI intensity is in agreement with conclusions of *Hines and Tarasick* [1994] that for vertical waves and chemical processes that occur on time scales much faster than a wave period, the phase difference between temperature and brightness must necessarily be 0° or 180°.

[22] The OH excitation process, however, occurs at a slower rate with longer characteristic time scale ($\tau_{O_3} = (k_1[H])^{-1} \simeq 6-10$ min) such that steady-state assumption is not valid for short-period waves with periods $\tau \sim \tau_{O_3}$. Negative wave temperature perturbations induce enhancements of O_3 production ($k_6\uparrow$ for $T\downarrow$) [*McDade et al.*, 1987]. The O_3 is then consumed slowly by the reaction leading to the production of excited OH; the rate of the excitation reaction, however, increases for positive temperature perturbations ($k_1\uparrow$ for $T\uparrow$). For waves presented in this paper, with period $\tau \leq \tau_{O_3}$, the emission is proportional to k_1, as it is rate-limited by the consumption of O_3 (and consequent OH production). It is this time dependence, coupled with the temperature dependence of k_1 in the OH production reaction, that causes the wave-induced OH emission to be in-phase with temperature perturbations and 180° out of phase with the OI layer for the modeled waves (Figures 2a, 2b, and 2c). For waves with period $\tau \gg \tau_{O_3}$ the emission will be proportional to k_6 rather than k_1 and will follow the production of O_3. If steady-state were falsely assumed by setting $\partial[O_3]/\partial t = 0$, the OI and OH emissions would have equal phase for the modeled waves, where both emission rates would enhance for negative temperature perturbations.

4. Conclusions

[23] One interpretation [*Munasinghe et al.*, 1998] of a short-period wave event reported by *Taylor et al.* [1995] has been modeled. Model results suggest that the ducted waves reach evanescence near the OH and OI airglow layers and perturb the two layers without significant vertical phase variations. These waves induce anti-phase OH and OI emissions, even though wave dynamics do not vary with altitude between the airglow layers. This results from the time and temperature dependencies of the OH excitation process. Wave characteristics and airglow phase variations strongly resemble those associated with gravity wave events categorized as mesospheric bores [e.g., *Taylor et al.*, 1995; *Smith et al.*, 2003]; however, present results do not reproduce the background airglow intensity jumps noted in the above cited observations.

[24] **Acknowledgments.** We would like to thank R. H. Picard, M. P. Hickey, M. J. Taylor, T. Y. Huang and E. M. Dewan for helpful discussions. We also thank G. R. Swenson and an anonymous reviewer for many useful comments and suggestions. This research was supported by NSF ATM-01-23020 and ATM-04-37140 grants to Penn State University.

References

Chimonas, G., H. M. Hauser, and R. D. Bennett (1996), The excitation of ducted modes by passing internal waves, *Phys. Fluids*, *8*(6), 1486–1505.

Dewan, E. M., and R. H. Picard (1998), Mesospheric bores, *J. Geophys. Res.*, *103*, 6295–6305.

Hedin, A. E. (1991), Extension of the MSIS thermospheric model into the middle and lower atmosphere, *J. Geophys. Res.*, *96*, 1159–1172.

Hines, C. O., and D. W. Tarasick (1994), Airglow response to vertically standing gravity waves, *Geophys. Res. Lett.*, *21*(24), 2729–2732.

Horinouchi, T. (2004), Simulated breaking of convectively generated mesoscale gravity waves and airglow modulation, *J. Atmos. Sol. Terr. Phys.*, *66*, 755–767.

LeVeque, R. J. (2002), *Finite Volume Methods for Hyperbolic Problems*, Cambridge Univ. Press, New York.

Liu, A. Z., and G. R. Swenson (2003), A modeling study of O_2 and OH airglow perturbations induced by atmospheric gravity waves, *J. Geophys. Res.*, *108*(D4), 4151, doi:10.1029/2002JD002474.

Makhlouf, U. B., R. H. Picard, and J. R. Winick (1995), Photochemical-dynamical modeling of the measured response of airglow to gravity waves: 1. Basic model for OH airglow, *J. Geophys. Res.*, *100*, 11,289–11,311.

Makhlouf, U. B., R. H. Picard, J. R. Winick, and T. F. Tuan (1998), A model for the response of the atomic oxygen 557.7 nm and the OH Meinel airglow to atmospheric gravity waves in a realistic atmosphere, *J. Geophys. Res.*, *103*, 6261–6269.

McDade, I. C., D. P. Murtagh, R. G. H. Greer, P. H. G. Dickinson, G. Witt, J. Stegman, E. J. Llewellyn, L. Thomas, and D. B. Jenkins (1986), ETON 2: Quenching parameters for the proposed precursors of $O_2(b^1\Sigma_g^+)$ and $O(^1S)$ in the terrestrial nightglow, *Planet. Space Sci.*, *34*(9), 789–800.

McDade, I. C., E. J. Llewellyn, D. P. Murtagh, and R. G. H. Greer (1987), ETON 5: Simultaneous rocket measurements of the OH Meinel ($\Delta v = 2$ sequence and (8,3) band emission profiles in the nightglow, *Planet. Space Sci.*, *35*(9), 1137–1147.

Munasinghe, G., H. Hur, T. Y. Huang, A. Bhattachryya, and T. F. Tuan (1998), Application of the dispersion formula to long-and short-period gravity waves: Comparisons with ALOHA-93 data and an analytical model, *J. Geophys. Res.*, *103*, 6467–6481.

Murtagh, D. P., G. Witt, J. Stegman, I. C. McDade, E. J. Llewellyn, F. Harris, and R. G. H. Greer (1990), An assessment of proposed $O(^1S)$ and $O_2(b^1\Sigma_g^+)$ nightglow excitation parameters, *Planet. Space Sci.*, *38*(1), 43–53.

Smith, M. S., M. J. Taylor, G. R. Swenson, C.-Y. She, W. Hocking, J. Baumgardner, and M. Mendillo (2003), A multidiagnostic investigation of the mesospheric bore phenomenon, *J. Geophys. Res.*, *108*(A2), 1083, doi:10.1029/2002JA009500.

Snively, J. B., and V. P. Pasko (2003), Breaking of thunderstorm-generated gravity waves as a source of short-period ducted waves at mesopause altitudes, *Geophys. Res. Lett.*, *30*(24), 2254, doi:10.1029/2003GL018436.

Swenson, G. R., and P. J. Espy (1995), Observations of 2-dimensional airglow structure and Na density from the ALOHA, October 9, 1993 "storm flight," *Geophys. Res. Lett.*, *22*(20), 2845–2848.

Swenson, G. R., and C. S. Gardner (1998), Analytical models for the response of the mesospheric OH* and Na layers to atmospheric gravity waves, *J. Geophys. Res.*, *103*, 6271–6294.

Swenson, G. R., J. Qian, J. M. C. Plane, P. J. Espy, M. J. Taylor, D. N. Turnbull, and R. P. Lowe (1998), Dynamical and chemical aspects of the mesospheric Na "wall" event on October 9, 1993 during the Airborne Lidar and Observations of Hawaiian Airglow (ALOHA) campaign, *Geophys. Res. Lett.*, *22*(20), 2845–2848.

Taylor, M. J., D. N. Turnbull, and R. P. Lowe (1995), Spectrometric and imaging measurements of a spectacular gravity wave event observed during the ALOHA-93 campaign, *Geophys. Res. Lett.*, *22*(20), 2849–2852.

V. P. Pasko and J. B. Snively, CSSL, Department of Electrical Engineering, Pennsylvania State University, 211B Electrical Engineering East, University Park, PA 16802, USA. (vpasko@psu.edu; jbs231@psu.edu)